Unexpected Formation of an Epoxide-Derived Multisubstrate Adduct Inhibitor on the Active Site of GAR Transformylase[†,‡]

Samantha E. Greasley,[§] Thomas H. Marsilje,[§] Hui Cai,[§,||] Stephen Baker,[⊥] Stephen J. Benkovic,[⊥] Dale L. Boger,[§] and Ian A. Wilson*[,§]

Departments of Molecular Biology and Chemistry and The Skaggs Institute for Chemical Biology, The Scripps Research Institute, 10550 North Torrey Pines Road, La Jolla, California 92037, and Department of Chemistry, The Pennsylvania State University, University Park, Pennsylvania 16802

Received July 17, 2001

ABSTRACT: Multisubstrate adduct inhibitors (MAI) of glycinamide ribonucleotide transformylase (GAR Tfase), which incorporate key features of the folate cofactor and the β-GAR substrate, typically exhibit K_i's in the picomolar range. However, these compounds have reduced bioavailability due to the incorporation of a negatively charged phosphate moiety that prevents effective cellular uptake. Thus, a folate analogue that is capable of adduct formation with the substrate on the enzyme active site could lead to a potent GAR Tfase inhibitor that takes advantage of the cellular folate transport systems. We synthesized a dibromide folate analogue, 10-bromo-10-bromomethyl-5,8,10-trideazafolic acid, that was an intermediate designed to assemble with the substrate β-GAR on the enzyme active site. We have now determined the crystal structure of the *Escherichia coli* GAR Tfase/MAI complex at 1.6 Å resolution to ascertain the nature and mechanism of its time-dependent inhibition. The high-resolution crystal structure clearly revealed the existence of a covalent adduct between the substrate β-GAR and the folate analogue ($K_i = 20$ μM). However, the electron density map surprisingly indicated a C10 hydroxyl in the adduct rather than a bromide and suggested that the multisubstrate adduct is not formed directly from the dibromide but proceeds via an epoxide. Subsequently, we demonstrated the in situ conversion of the dibromide to the epoxide. Moreover, synthesis of the authentic epoxide confirmed that its inhibitory, time-dependent, and cytotoxic properties are comparable to those of the dibromide. Further, inhibition was strongest when the dibromide or epoxide is preincubated with both enzyme and substrate, indicating that inhibition occurs via the enzyme-dependent formation of the multisubstrate adduct. Thus, the crystal structure revealed the successful formation of an enzyme-assembled multisubstrate adduct and highlighted a potential application for epoxides, and perhaps aziridines, in the design of efficacious GAR Tfase inhibitors.

The folate-dependent enzymes, dihydrofolate reductase (DHFR),[1] thymidylate synthase (TS), glycinamide ribonucleotide transformylase (GAR Tfase), and 5-aminoimidazole-4-carboxamide ribonucleotide transformylase (AICAR Tfase), have long been established as viable targets for antineoplastic intervention. However, despite considerable attempts to design efficacious antifolates against these enzymes, there remains a paucity of clinically useful compounds. We have focused our attention on the design of inhibitors against the two folate-dependent enzymes of the de novo purine biosynthesis pathway, GAR Tfase and AICAR Tfase. Both of these enzymes utilize the cofactor 10-formyltetrahydrofolate (10-formyl-THF) to catalyze the formylation of glycinamide ribonucleotide (GAR) (*1*, *2*) and 5-aminoimidazole-4-carboxamide ribonucleotide (AICAR) (*3*), respectively. In particular, one of our major goals has been to design lead compounds capable of forming an enzyme-assembled multisubstrate adduct inhibitor (MAI) (*4*) through examination of the crystal structures of GAR Tfase (*5*−*9*) and, more recently, AICAR Tfase (*10*). In this way, delivery of the appropriate folate analogues to cells is not complicated by the presence of charged moieties that inhibit cell entry.

Multisubstrate adduct inhibitors (MAI), such as BW1476-U89 (*7*, *11*) and thio-GAR-dideazafolate (TGDDF) (*12*), which contain key components of both the folate cofactor and substrate, β-GAR, have demonstrated superb potency against GAR Tfase, with K_i's in the picomolar range (*11*, *12*). However, these compounds are large and complex, and

[†] This work was supported by NIH Grant CA63536 to I.A.W., D.L.B., and S.J.B. This is Publication 14284-MB from The Scripps Research Institute.

[‡] The coordinates have been deposited with the Protein Data Bank with ID code 1JKX.

* To whom correspondence should be addressed. E-mail: wilson@scripps.edu. Phone: (858) 784-9706. Fax: (858) 784-2980.

[§] The Scripps Research Institute.

[||] Present address: The R. W. Johnson Pharmaceutical Research Institute, 3210 Merryfield Row, San Diego, CA 92121.

[⊥] The Pennsylvania State University.

[1] Abbreviations: DHFR, dihydrofolate reductase; TS, thymidylate synthase; GAR Tfase, glycinamide ribonucleotide transformylase; AICAR Tfase, aminoimidazolecarboxamide ribonucleotide transformylase; 10-formyl-THF, 10-formyltetrahydrofolate; MAI, multisubstrate adduct inhibitor; 10-formyl-TDAF, 10-formyl-5,8,10-trideazafolic acid; DDATHF, 6(*R*,*S*)-5,10-dideaza-5,6,7,8-tetrahydrofolic acid; 5-DATHF, 5-deazatetrahydrofolate; MPD, methyl pentanediol; PDB, Protein Data Bank; fDDF, 10-formyldideazafolate.

10.1021/bi011482+ CCC: $20.00
Published on Web 10/18/2001

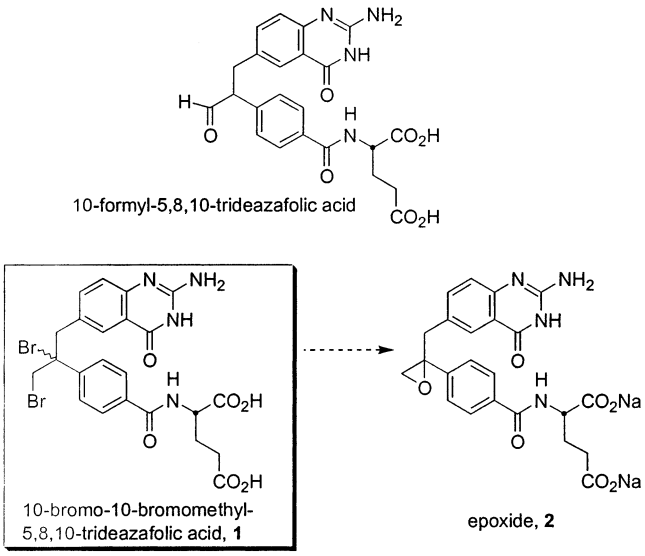

FIGURE 1: Folate−base inhibitors of GAR Tfase. The dibromide **1** (boxed compound), a functionalized analogue of 10-formyl-5,8,-10-trideazafolic acid, forms a multisubstrate adduct with β-GAR via epoxide **2**.

the presence of the negatively charged phosphate moiety prevents effective cellular uptake; thus, reduced bioavailability and general cytotoxicity hinder the clinical application of such inhibitors. Consequently, if a chemically simpler folate compound can be synthesized which has the capacity to sequester the natural substrate, β-GAR, within the enzyme active site, we could potentially assemble a potent GAR Tfase and/or AICAR Tfase adduct inhibitor of clinical utility. Further, we could also take advantage of the cells own folate uptake systems via the reduce folate carrier and folate binding protein (*13*). Indeed, GAR Tfase was previously shown to be capable of in situ MAI formation (*14*); unfortunately, the folate analogue, N^{10}-bromoacetyl dideazafolate, was too reactive and unstable to be adopted as a drug (*11*).

The compound 10-bromo-10-bromomethyl-5,8,10-trideazafolic acid (dibromide, **1**) (*15*), a functionalized analogue of 10-formyl-5,8,10-trideazafolic acid (10-formyl-TDAF) (*4*) (Figure 1), although not a particularly potent inhibitor toward GAR Tfase (K_i of 20 μM), was observed to exhibit time-dependent inhibition (<20% activity remaining after 460 min, Figure 2A) (*15*). It was previously proposed that this time-dependent inhibition was a result of the formation of a multisubstrate adduct with the substrate, β-GAR, and/or alkylation of an active site residue by the inhibitor. Additional inhibition studies, in the presence and absence of β-GAR, strongly favored the formation of a multisubstrate adduct (*15*).

The high-resolution crystal structure of *Escherichia coli* (*E. coli*) GAR Tfase, crystallized in the presence of the dibromide inhibitor, **1**, and substrate, β-GAR, was determined to 1.6 Å resolution to ascertain the exact nature of the time-dependent enzyme inhibition. Subsequently, an authentic epoxide compound was synthesized, and its inhibitory properties were evaluated, to substantiate the existence of the C10 hydroxyl of the MAI observed in the crystal structure, thus providing an additional perspective for the design of antifolates against de novo purine biosynthesis enzymes.

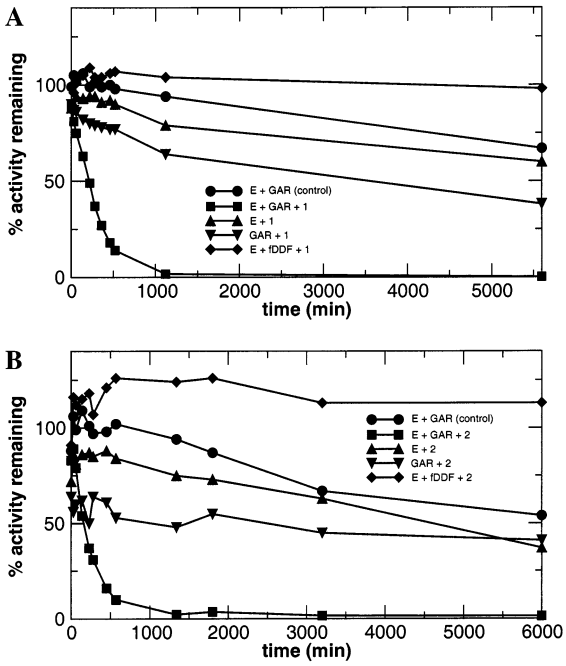

FIGURE 2: Plot of GAR Tfase activity vs time for different incubation conditions of (A) the dibromide analogue **1** and (B) the epoxide analogue **2**. Assay conditions: 2 nM *pur*N GAR Tfase (E), 10 μM inhibitor (**1** or **2**), 20 μM fDDF, 50 μM GAR, and 2 min preincubation.

MATERIALS AND METHODS

Materials. Luria broth and agar were obtained from Life Technologies, Gaithersburg, MD. All common buffers and reagents were purchased from Sigma-Aldrich Corp., St. Louis, MO. The substrate (α,β)-GAR was synthesized as described previously (*16*).

Protein Preparation and Purification. *E. coli* GAR Tfase was prepared as reported previously (*2*, *9*). Approximately 25 mg of GAR Tfase can be recovered per 1 L preparation of cells and purified to 98% homogeneity, as assessed by SDS−PAGE. Purified enzyme was stored at 4 °C, at a concentration of 2.6 mg/mL in 50 mM Tris-HCl, pH 7.5, and 1 mM EDTA. The dibromide inhibitor was dissolved in 100% DMSO and added to the dilute protein to give a 10-fold molar excess. The substrate, (α,β)-GAR, was dissolved in water and added in 1.2-fold molar excess to the protein/inhibitor solution and incubated overnight at 4 °C before concentrating to 10 mg/mL suitable for crystallization experiments.

Crystallization and Data Collection. The protein/ligand complex was crystallized by the method of vapor diffusion in sitting drops (*17*). The protein solution was mixed with an equal volume (1.8 μL) of precipitating solution and left to equilibrate at 22 °C. Initial crystals were obtained after 1 week from 22% polyethylene glycol (PEG) 3350, 0.15 M calcium chloride, 4% MPD (v/v), and 0.1 M imidazole malate (pH 7.4). These crystals were then macroseeded into 14% PEG 3350, 0.15 M calcium chloride, 4% MPD, and 0.1 M imidazole malate (pH 7.4) that resulted in large (0.4 mm × 0.2 mm × 0.05 mm) platelike crystals, which were typically multilayered.

Owing to the thin nature of these crystals, data collection was only possible at a synchrotron source. Data were collected to 1.6 Å resolution from a single crystal at −178

Table 1: Data Collection and Refinement Statistics

space group	*P*1
unit cell dimensions (Å; deg)	$a = 55.14$, $b = 56.01$, $c = 76.13$; $\alpha = 80.83$, $\beta = 71.71$, $\gamma = 83.69$
no. of molecules per au	4
resolution range (Å)	30−1.6 (1.64−1.60)[a]
no. of unique reflections	106828 (6398)
completeness (%)	94.4 (76.4)
multiplicity	1.9 (1.5)
average I/σ	6.2 (2.2)
R_{sym} [b] (%)	5.0 (32.5)
refinement	
resolution range (Å)	30−1.6
data cutoff	$F_o > 0\sigma$
reflections (test set)	106744 (10690)
protein atoms	6469
water molecules	607
inhibitor atoms	208
R_{cryst}:R_{free} [c] (%)	22.1:24.3
Ramachandran plot (%)	
most favored	91.2
additionally allowed	8.6
generously allowed	0.3
disallowed	0.0

[a] Numbers in parentheses refer to the highest resolution shell. [b] $R_{merge} = (\sum_h\sum_i|I_i(h) - \langle I(h)\rangle|/\sum_h\sum_i I_i(h)) \times 100$, where $\langle I(h)\rangle$ is the mean of the $I(h)$ observation of reflection h. [c] $R_{cryst} = (\sum_h|F_o - F_c|/\sum_h F_o) \times 100$, where F_o and F_c are the observed and calculated structure factors, respectively. R_{free} is computed as for R_{cryst} but with the test set of reflections only.

°C on beam line 9-1 at Stanford Synchrotron Radiation Laboratory, using a MAR345 imaging plate. A single crystal was cryocooled by mounting in a loop (Hampton Research, Laguna Hills, CA) that was quickly dragged through a solution of mother liquor, where the MPD concentration had been raised from 4% to 10%, before cryocooling directly in the liquid nitrogen stream.

Data were processed with MOSFLM (*18*) and scaled with SCALA (*19*) and programs from the CCP4 suite (*20*). The crystals belong to space group *P*1, with unit cell dimensions $a = 55.14$ Å, $b = 56.01$ Å, $c = 76.13$ Å, $\alpha = 80.83°$, $\beta = 71.71°$, and $\gamma = 83.69°$. Calculation of the Matthews coefficient ($V_m = 2.5$) (*21*) suggested four molecules per asymmetric unit. Data statistics are given in Table 1.

Structure Solution and Refinement. The structure was determined using molecule 1 from the refined structure of GAR Tfase in complex with 10-formyl-TDAF (PDB file 1C2T) (*9*) as the search model for molecular replacement using the program EPMR (*22*). All water molecules, inhibitor, and substrate were removed from the model. The search was conducted with data from 10.0 to 3.5 Å, and all four molecules were found in a single EPMR run, resulting in an *R*-value of 36.4% and a correlation coefficient (cc) of 64.2 (incorrect solution has an *R*-value = 45.8% and cc = 42.2).

Refinement was carried out using the program CNS (*23*) with overall anisotropic temperature factor correction (where $B_{11} = -0.6$ Å^2, $B_{22} = -4.0$ Å^2, $B_{33} = 3.4$ Å^2, $B_{12} = -0.5$ Å^2, $B_{23} = -1.8$ Å^2, and $B_{13} = 2.7$ Å^2) and bulk solvent correction applied at each round of refinement (*24*). A test set of 10% of reflections was omitted for the calculation of R_{free} (*25*). The R_{cryst} and R_{free} values after rigid body refinement from 30 to 3.5 Å resolution were 38.1% and 38.1%, respectively. Simulated annealing, followed by 200 cycles of conventional positional refinement, was performed to 1.6 Å, using noncrystallographic symmetry (ncs) restraints of 300 and 100 kcal mol^{-1} for main-chain and side-chain atoms, respectively (all residues). After individual temperature factor refinement, R_{cryst} and R_{free} were 30.6% and 31.3%, respectively. Electron density maps (σ_A-weighted $3F_o - 2F_c$, $2F_o - F_c$, and $F_o - F_c$) calculated at this stage clearly revealed electron density in the active site of each molecule for the folate inhibitor, with distinct density connecting to the primary amine of β-GAR (Figure 3).

To establish which form of the inhibitor was bound, a number of models were refined, including both the (10*R*) and (10*S*) diastereomers, inhibitor minus the primary bromide, a version with the primary bromide removed and the tertiary bromide replaced by a methyl group, and the (10*S*) form covalently linked to β-GAR via removal of the primary bromide, with either a tertiary bromide or hydroxyl group. All inhibitor models were built in InsightII (MSI, San Diego, CA), and topology and parameter files required for CNS refinement were generated by XPLO2D (*26*). The electron density calculated from each model strongly suggested that the best fit to the electron density was observed for the covalently linked adduct containing a (10*S*)-C10 hydroxyl. All subsequent refinements were performed with this derivative. Cycles of conventional positional refinement and individual *B*-value refinement using all data from 30.0 to 1.6 Å were alternated with manual rebuilding with O (*27*). Density modification with 4-fold averaging, solvent flattening, and histogram matching was employed in DM (*28*) to produce improved electron density maps to facilitate model building of the more disordered regions (typically residues 112−132, 140−146, 154−168, and 191−209) (Figure 4). The loop containing residues 141−145 required the most rebuilding as it adopts a conformation different from that observed in other folate-bound complex structures (*5*, *6*, *9*). Ncs restraints were released for the more disordered regions of the structure (listed above) and were never applied to the inhibitor/substrate adduct. In the later stages of refinement, water molecules were fit using a combination of the automated water picking routine in CNS (442 waters) and manual addition of a further 165 waters during the final rebuilding cycle. During the last round of refinement, all ncs restraints were released, resulting in a final R_{cryst} and R_{free} of 22.1% and 24.3%, respectively. The Ramachandran values of the model are excellent as assessed by PROCHECK (*29*) (Table 1). The model was compared to the following structures in the PDB: ternary complex with β-GAR and 10-formyl-TDAF [1C2T (*9*)], ternary complex with β-GAR and 5-DATHF [1CDE (*5*)], complex with BW1476U89 [1GAR (*7*)], low pH phosphate-bound structures [1GRC and 1CDD (*5*, *6*)], E70A phosphate-bound structures (*8*) at low pH (2GAR) and high pH (3GAR).

*Synthesis of Epoxide **2***. The synthesis of the epoxide **2** is shown in Scheme 1. The known diacid **5** (*15*) was esterified to provide the dimethyl ester **6** by treatment with catalytic H_2SO_4−CH_3OH (25 °C, 12 h). The dimethyl ester protection was chosen in order to allow saponification of the esters during the base-catalyzed epoxide closure reaction, releasing the glutamate as a carboxylic acid salt. Compound **6** was converted to its corresponding bromohydrin **7** by reaction with 1 equiv of *N*-bromosuccinimide (NBS) in aqueous dioxane at room temperature overnight. Finally, the bromohydrin **7** was treated with 3 equiv of lithium hydroxide in aqueous CH_3OH at room temperature overnight to simulta-

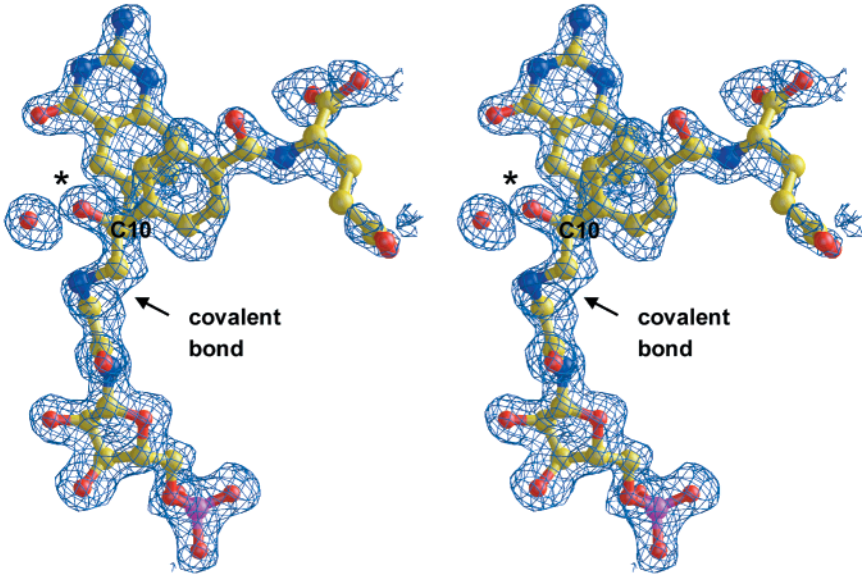

FIGURE 3: Stereoview of the initial, unbiased, electron density with superimposed final coordinates for the multisubstrate adduct formed between β-GAR and the dibromide. The density shown is from a $3F_o - 2F_c$ σ_A-weighted map contoured at 1.2σ and clearly shows connecting density between the substrate and inhibitor and insufficient electron density for a tertiary bromide (*). The C10 carbon has been labeled for clarity. Atoms are colored according to atom type.

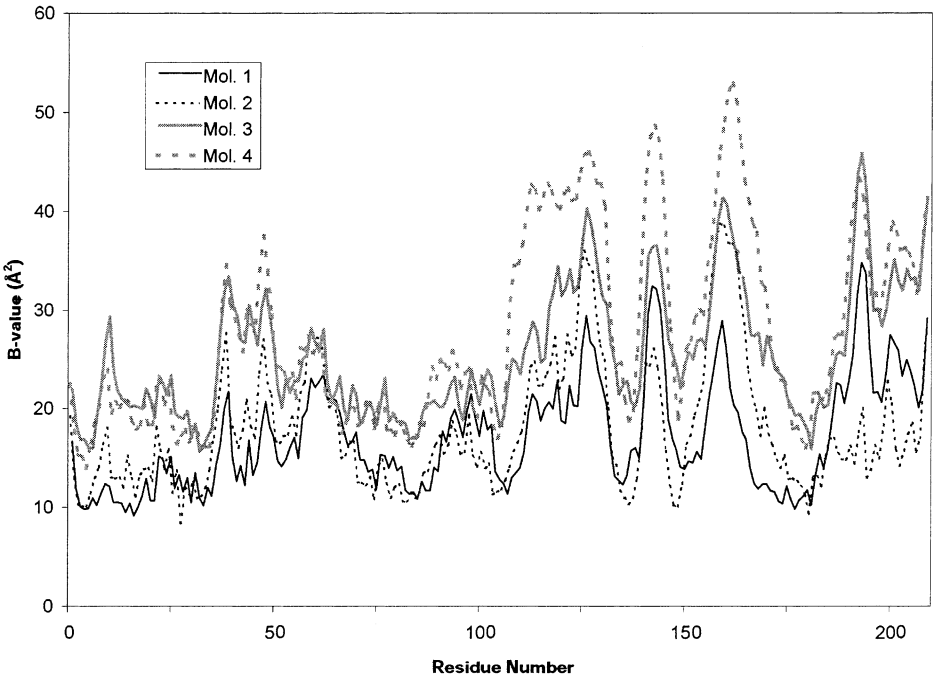

FIGURE 4: Plot of *B*-values vs residue number for Cα atoms of GAR Tfase molecules 1−4. The plot highlights the previously identified disordered regions of the structure (residues 112−132, 140−146, 154−168, and 191−209). In this study, molecules 3 and 4 have higher average *B*-values than molecules 1 and 2.

neously close the epoxide ring and saponify the two methyl esters forming the dilithium salt of the epoxide **2**.

*Dimethyl N-[4-[3-(2-Amino-3,4-dihydro-4-oxoquinazolin-6-yl)prop-1-en-2-yl]benzoyl]-L-glutamate (**6**).* A solution of **5** (*15*) (20.0 mg, 0.018 mmol) in CH_3OH (4 mL) was treated with concentrated H_2SO_4 (3 drops). The reaction mixture was allowed to stir at room temperature overnight. The reaction mixture was poured into saturated aqueous $NaHCO_3$ (20 mL) and extracted with EtOAc (3 × 30 mL). The combined organic layers were washed with saturated aqueous NaCl (1 × 30 mL), dried over Na_2SO_4, and concentrated to provide **6** (17.0 mg, quantitative) as a pale yellow solid: ^{1}H NMR (CD_3OD, 400 MHz) δ 7.85 (s, 1H), 7.74 (d, J = 8.5 Hz, 1H), 7.55 (d, J = 8.5 Hz, 1H), 7.25 (d, J = 7.6 Hz, 2H), 7.19 (d, J = 7.6 Hz, 2H), 5.60 (s, 1H), 5.24 (s, 1H), 4.63−4.58 (m, 1H), 3.96 (s, 2H), 3.72 (s, 3H), 3.62 (s, 3H), 2.46 (t, J = 7.5 Hz, 2H), 2.33−2.21 (m, 1H), 2.12−2.00 (m, 1H); MALDI-FTMS (DHB) *m/z* 479.1929 ($M + H^+$, $C_{25}H_{26}N_4O_6$ requires 479.1931).

*Dimethyl (2RS)-N-[4-[3-(2-Amino-3,4-dihydro-4-oxoquinazolin-6-yl)-2-bromo-1-hydroxyprop-2-yl]benzoyl]-L-glutamate (**7**).* A solution of **6** (34.0 mg, 0.071 mmol) in 1,4-dioxane (4 mL) and H_2O (2 mL) was treated with *N*-bromosuccinimide (13.0 mg, 0.073 mmol, 1.0 equiv). The reaction mixture was allowed to stir at room temperature overnight. The reaction mixture was poured into distilled H_2O

Scheme 1

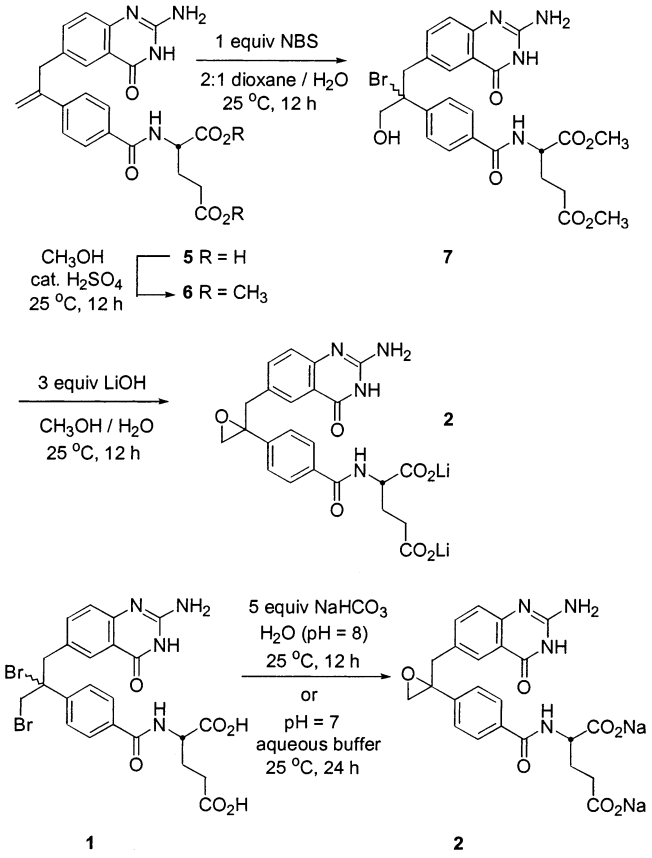

(20 mL) and extracted with EtOAc (3 × 30 mL). The combined organic layers were washed with saturated aqueous NaCl (1 × 30 mL), dried over Na_2SO_4, and concentrated. The film isolated was triturated with CH_2Cl_2 + hexanes and concentrated to provide **7** (32 mg, 79%) as a white solid: ^{1}H NMR (CD_3OD, 250 MHz) δ 7.85−7.72 (m, 2H), 7.76 (d, J = 8.8 Hz, 2H), 7.46 (d, J = 8.0 Hz, 2H), 7.49−7.42 (m, 1H), 4.64−4.56 (m, 1H), 3.72 (s, 3H), 3.75−3.64 (m, 4H), 3.61 (s, 3H), 2.46 (t, J = 7.1 Hz, 2H), 2.35−2.20 (m, 1H), 2.17−2.01 (m, 1H); MALDI-FTMS (DHB) *m/z* 597.0931 (M + Na^+, $C_{25}H_{27}BrN_4O_7$ requires 597.0955).

*(2RS)-N-[4-[3-(2-Amino-3,4-dihydro-4-oxoquinazolin-6-yl)-1,2-(ethylene oxide)prop-2-yl]benzoyl]-*L*-glutamic Acid Dilithium Salt (**2**).* A solution of **7** (10.0 mg, 0.017 mmol) in CH_3OH (1 mL) and H_2O (1 drop) was treated with LiOH−H_2O (2.2 mg, 0.052 mmol, 3.0 equiv). The reaction mixture was allowed to stir at room temperature overnight before the reaction mixture was concentrated. The film isolated was triturated with and concentrated from CH_3CN (1×) and CH_2Cl_2 + hexanes (1×) to cleanly provide **2** dilithium salt + 1 equiv of LiBr (9.8 mg) as a white solid. The inorganic impurities were removed to generate an analytical sample using Sephadex LH-20 (100 g, CH_3OH eluent) gel filtration chromatography: ^{1}H NMR (CD_3OD, 250 MHz) δ 7.86 (s, 1H), 7.82 (d, J = 8.4 Hz, 2H), 7.44 (d, J = 8.4 Hz, 2H), 7.35 (d, J = 8.5 Hz, 1H), 7.07 (d, J = 8.4 Hz, 1H), 4.40−4.35 (m, 1H), 3.51 (d, J = 14.8 Hz, 1H), 2.96 (d, J = 5.0 Hz, 1H), 2.73 (d, J = 5.4 Hz, 1H), 2.29 (t, J = 6.9 Hz, 2H), 2.26−2.05 (m, 2H); MALDI-FTMS (DHB) *m/z* 467.1563 (M + H^+, $C_{23}H_{22}N_4O_7$ requires 467.1567).

*Conversion of Dibromide **1** to Epoxide **2**.* To establish the feasibility of in situ epoxide generation from compound **1**, the dibromide (*15*) was stirred in either mildly basic (pH 8) distilled water which contained 5 equiv of $NaHCO_3$ overnight or pH 7 phosphate buffer for 24 h (Scheme 1). After concentration in vacuo, ^{1}H NMR and high-resolution mass spectroscopy indicated the surprisingly facile and quantitative conversion of the dibromide to the disodium salt of epoxide **2**. This indicates that compound **1** is completely converted to epoxide **2** under the aqueous assay conditions and conditions similar to the crystallization media. In fact, the synthesis of epoxide **2** via the mild reaction of dibromide **1** is a more efficient synthetic route than via the bromohydrin dimethyl ester intermediate discussed above.

*(2RS)-N-[4-[3-(2-Amino-3,4-dihydro-4-oxoquinazolin-6-yl)-1,2-(ethylene oxide)prop-2-yl]benzoyl]-*L*-glutamic Acid Disodium Salt (**2**).* A solution of **1**−CF_3CO_2H (*15*) (4.0 mg, 5.5 μmol) in distilled H_2O (3 mL) was treated with solid $NaHCO_3$ (2.3 mg, 28 μmol, 5.0 equiv). The reaction mixture was allowed to stir at room temperature overnight before the reaction mixture was concentrated. The film isolated was triturated with and concentrated from CH_3CN (1×) to cleanly provide **2** disodium salt + 2 equiv of NaBr + 1 equiv of sodium trifluoroacetate (4.7 mg) as a white solid: ^{1}H NMR (CD_3OD, 250 MHz) δ 7.86 (s, 1H), 7.81 (d, J = 8.7 Hz, 2H), 7.43 (d, J = 8.7 Hz, 2H), 7.39 (d, J = 8.7 Hz, 1H), 7.08 (d, J = 8.7 Hz, 1H), 4.40−4.34 (m, 1H), 3.55 (d, J = 15.4 Hz, 1H), 2.98 (d, J = 5.4 Hz, 1H), 2.74 (d, J = 5.7 Hz, 1H), 2.29 (t, J = 7.5 Hz, 2H), 2.26−2.05 (m, 2H); MALDI-FTMS (DHB) *m/z* 489.1373 (M + Na^+, $C_{23}H_{22}N_4O_7$ requires 489.1386). Alternatively, **1**−CF_3CO_2H (*15*) (7.8 mg, 10.8 μmol) was partially dissolved in pH 7 aqueous phosphate buffer (1 mL, 0.05 M potassium phosphate monobasic−sodium hydroxide buffer). This reaction mixture was allowed to stir at room temperature for 24 h before the reaction mixture was concentrated. The inorganic salts were removed via Sephadex LH-20 (100 g, CH_3OH as eluent) gel filtration chromatography to generate compound **2** (5.0 mg, 91%): ^{1}H NMR (CD_3OD, 250 MHz) δ 7.86 (s, 1H), 7.81 (d, J = 8.4 Hz, 2H), 7.42 (d, J = 8.1 Hz, 2H), 7.45−7.39 (m, 1H), 7.09 (d, J = 8.4 Hz, 1H), 4.40−4.34 (m, 1H), 3.59 (d, J = 15.1 Hz, 1H), 2.98 (d, J = 4.0 Hz, 1H), 2.75 (d, J = 5.0 Hz, 1H), 2.30 (t, J = 6.9 Hz, 2H), 2.26−1.96 (m, 2H).

Biological Testing. Time-dependent inhibition of GAR Tfase by the epoxide **2** was examined as described previously (*4*), and results are presented in Figure 2B. Cytotoxicity testing was also performed as described previously (*4*) (Table 2).

Table 2: Cytotoxic Activity (IC_{50}, μM)[a]

agent	L1210[b]	CCRF-CEM[b]
(6*R*)-DDATHF	>225, 0.07	>225, 0.05
methotrexate	0.05, 0.05	0.06, 0.07
1	50, 40	60, 50
2	not tested	30, 30

[a] Dialyzed FBS, RPMI-1640 medium. [b] With (+) hypoxanthine, (−) hypoxanthine.

RESULTS AND DISCUSSION

X-ray Structure Determination. E. coli GAR Tfase was cocrystallized in the presence of its substrate, β-GAR, and the folate-based inhibitor, 10-bromo-10-bromomethyl-5,8,-10-trideazafolic acid, from polyethylene glycol in the space

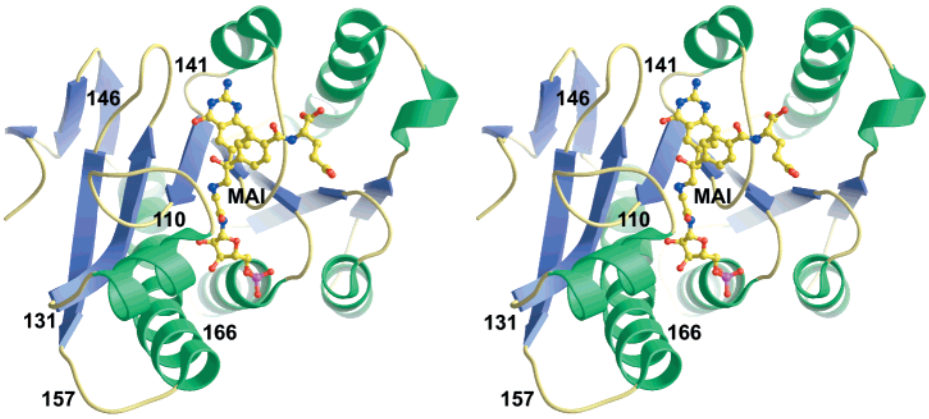

FIGURE 5: Stereoview of a ribbon figure of GAR Tfase showing the final coordinates for the multisubstrate adduct (MAI) formed between β-GAR and the dibromide. The labeled regions correspond to loops that contain the more disordered regions of the structure, as seen in Figure 4. Helices are shown in green, β-strands in blue, and connecting loops in yellow. The MAI is shown as a ball-and-stick representation and is colored by atom type.

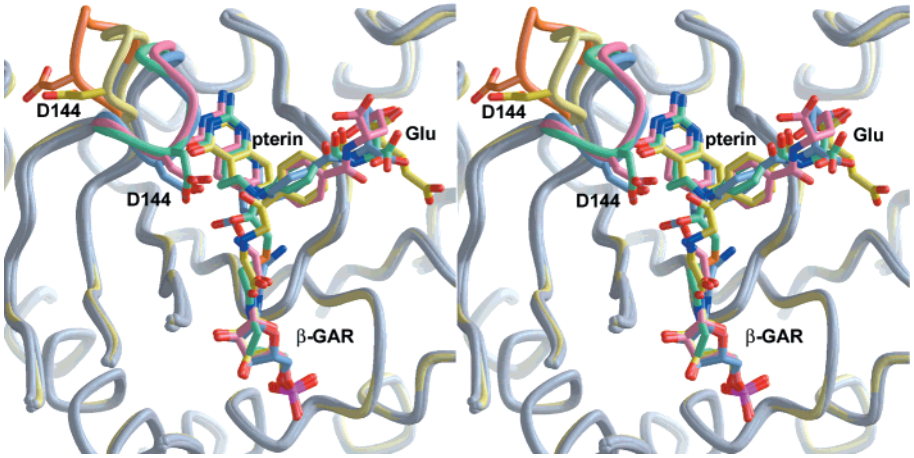

FIGURE 6: Stereoview of the active site of GAR Tfase illustrating the different conformations of the flexible "folate-dependent" loop, 141−146, and substrate/inhibitor structures. Superposition of the coordinates was performed in ProFit using core residues (see Table 3). The structure in yellow is the current structure while all other models are colored gray, except for the flexible loop (Asp 144 is also shown) which is colored pale blue (10-formyl-TDAF), mint green (molecule 1 of BW1476U89), pink (5-DATHF), and orange (E70A, pH 7.5). The carbon atoms of each substrate/inhibitor are colored the same as the corresponding loop. Only a slice through the active site region is shown for clarity. The pterin and glutamate moieties of the folate analogues are highlighted, as is the substrate, β-GAR.

group *P*1, with four molecules in the asymmetric unit. Molecule 1 of the 2.1 Å structure of GAR Tfase in complex with 10-formyl-TDAF (PDB file 1C2T) (*9*) was used as the search model for structure determination by molecular replacement. The structure was refined to 1.6 Å (the highest resolution GAR Tfase structure so far) and contains all residues (except the three C-terminal residues, 210−212, which are disordered) and one molecule of the multisubstrate adduct that is formed between the substrate and compound **1** (Figure 5) for each of the four molecules in the asymmetric unit. Data collection and refinement statistics are summarized in Table 1.

Overall Structure. The topology of this enzyme is very similar to those reported previously (*5*−*9*) and, not surprisingly, exhibits the greatest similarity to those structures determined above pH 6.8 (*5*, *8*, *9*). High pH is necessary for formation of an ordered loop−helix for residues 110−131 (Figure 5). Additionally, the enzyme is monomeric rather than in the dimeric form observed at lower pH (*5*−*7*). The structures for each of the four molecules in the asymmetric unit are very similar (rms deviations for all Cα atoms for molecules 2, 3, and 4 are 0.2, 0.3, and 0.5 Å, respectively), with molecule 4 showing the greatest deviation. In general, molecules 3 and 4 are more disordered than molecules 1 and 2, as reflected in the average *B*-values (18.3, 19.2, 26.2, and 28.7 Å^2 for all protein atoms in molecules 1−4, respectively) (Figure 4). The *B*-values of each molecule reveal a profile comparable to all other reported structures, with regions 110−131 [pH-dependent loop−helix (*8*)], 141−146 [containing the catalytic residue, Asp 144 (*7*, *30*)], and 157−166, and the C-terminal residues 191−209 exhibiting the highest thermal parameters.

Although the loop containing Asp 144 is flexible, as exhibited by high *B*-values in all known GAR Tfase structures, it appears to exist in three discrete conformations: flipped into the active site, flipped out of the active site, or in a position between these two extremes. To date, all structures that have a folate analogue inhibitor bound [BW1476U89 (*7*), 5-DATHF (*5*), and 10-formyl-TDAF (*9*)] display the same "in between" conformation of this loop, independent of the pH of crystallization (Figure 6), suggesting that the loop becomes fixed by two hydrogen bond interactions from the protein main chain to the pteridine ring system (O of Thr 140 to N3 and NH of Asp 144 to O4). In the absence of inhibitor [phosphate-bound structures (*5*, *6*) and the E70A, high and low pH structures (*8*)], the loop

Table 3: rms Deviations (Å) of Molecule 1 of the MAI Complex with Other *E. coli* GAR Tfase Structures

		region (Cα atoms)		
model	core[a]	110−131	141−146	157−166
10-f-TDAF[b] molecule 1	0.3	0.7	4.0	0.9
10-f-TDAF molecule 2	0.3	0.7	4.0	0.7
BW1476U89[c] molecule 1	0.4	−[h]	3.6	2.7
BW1476U89 molecule 2	0.3	−	3.4	1.4
5-DATHF[d]	0.4	0.7	3.7	0.8
apo[e] molecule 1	0.5	−	4.3	2.4
apo molecule 2	0.6	−	1.7	1.8
E70A,[f] pH 3.5	0.6	−	5.6	2.3
E70A,[g] pH 7.5	0.4	0.8	1.7	1.6

[a] Molecules were superimposed on structurally well conserved core residues (1−109 + 132−140 + 147−156 + 167−190), excluding flexible regions, using ProFit (A. C. R. Martin, SciTech Software). [b] PDB file 1C2T. [c] PDB file 1GAR. [d] PDB file 1CDE. [e] PDB file 1GRC. [f] PDB file 2GAR. [g] PDB file 3GAR. [h] Residues 110−131 are missing or disordered in these structures.

adopts two additional conformations, flipped into or out of the binding pocket, possibly as a result of crystal packing interactions. It has been postulated that the ordering of this loop helps to prepare the active site for the formyl transfer reaction (*8*).

Interestingly, the electron density for this loop in the MAI structure clearly shows that these residues adopt a flipped out conformation (Figure 6, Table 3), as observed in molecule 2 of the apo crystal structures (*5*, *6*) and in the apo E70A high pH structure (*8*), rather than the orientation seen in the other folate-bound structures. Residues 142−145 form a type I β-turn, and the loop is predominantly held in position through hydrogen bond interactions with water molecules. The effect that this loop rearrangement, and concurrent removal of the two hydrogen bond interactions, has on the binding of the quinazoline ring of the dibromide **1** is discussed below.

Structure of the Multisubstrate Adduct. The advantage of higher resolution data is that the chemical identification and conformation of the actual bound ligand adduct can be assessed with considerable confidence. This point was demonstrated beautifully when the first electron density maps for this structure were calculated. We could unambiguously build a model for almost all of the dibromide inhibitor (except the glutamate moiety) and all atoms of the β-GAR substrate, including identification of the ribose ring pucker as C(1) exo (Figure 3). In particular, we observed formation of a covalent bond between the amine of β-GAR and compound **1**. However, the electron density around the tertiary bromide was not at the level expected for an electron dense atom, and the predicted bond length (ca. 1.5 Å) connecting to the adjacent carbon was shorter than that typically observed for a carbon−bromine bond (1.94 Å). The structure suggested the presence of a C10 hydroxyl, and a number of different models were refined (see Materials and Methods) to establish the nature of the atoms around the C10 position of the inhibitor. Refinement convincingly concurred that a C10 hydroxyl was present and, hence, the electrophilic species responsible for the β-GAR alkylation within the GAR Tfase active site; furthermore, the alkylation of an AICAR Tfase active site residue (*15*) by the same inhibitor would most likely have come from an epoxide **2** rather than the original dibromide **1**. This mechanism would require the facile, in situ conversion of the dibromide to the epoxide followed by its effective enzyme inhibition or inactivation. Presumably, the sequence of epoxide formation arises by bromonium ion formation, **3**, followed by water addition to the bromonium ion to provide an intermediate bromohydrin **4**, and finally closure to the epoxide **2** (Scheme 2). A small number of reports have described the conversion of similar dibromides to their bromohydrin (*31*), followed by closure to the corresponding epoxide (*32*−*35*). To our knowledge, all such reports utilized more vigorous, basic conditions for this conversion than that required of the in situ conversion of dibromide **1** to epoxide **2**. We have successfully demonstrated the conversion of dibromide **1** to the epoxide **2** under aqueous assay conditions (see Materials and Methods). To establish the viability of this in situ generation of the putative epoxide **2**, an authentic sample of **2** was independently prepared and its properties were established (see Materials and Methods). Although it is expected that the epoxide-opening reaction proceeds via a trans-planar attack of the GAR amine nucleophile, interestingly, the covalent adduct exhibits a dihedral angle of only 52°. This suggests that a confomational rearrangement may occur following formation of the MAI.

Scheme 2

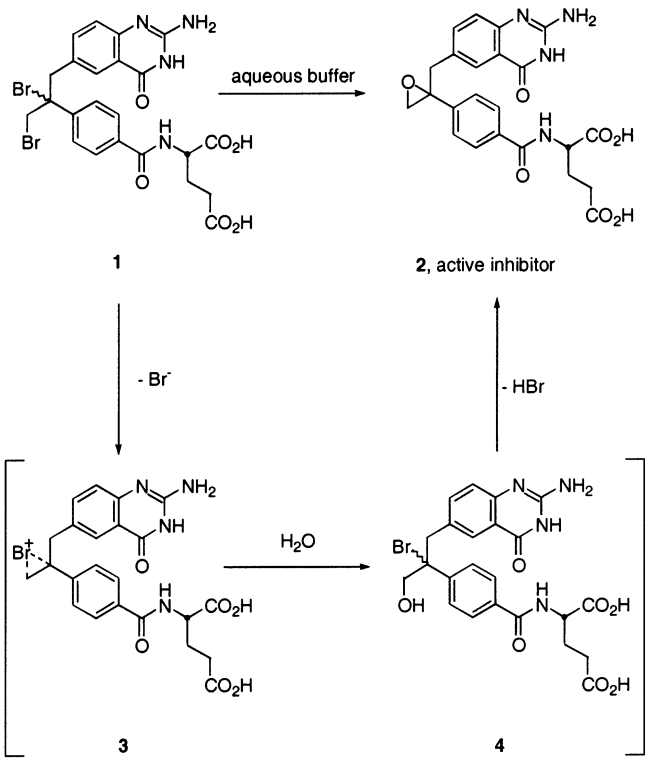

Ligand Interactions. The binding of the multisubstrate adduct in the enzyme active site is similar to that observed in other GAR Tfase complex structures deposited in the PBD, namely, the multisubstrate analogue inhibitor BW1476U89 (*7*), the 5-DATHF-β-GAR (*5*), and the 10-formyl-TDAF-β-GAR complexes (*9*) (Figure 6). The phosphate moiety, in particular, shows the greatest structural overlap, as this region is involved in extensive hydrogen-bonding interactions (Figure 7) and is additionally stabilized by the helix dipole moment (*6*). The ribose portion of β-GAR presents different interactions to the protein in each of the four molecules in the asymmetric unit. These differences arise from the change

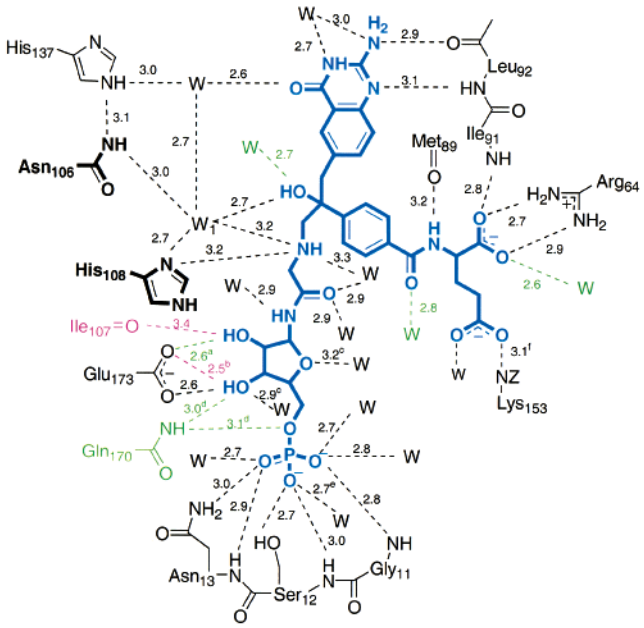

FIGURE 7: Potential hydrogen bond interactions between GAR Tfase and the enzyme-assembled multisubstrate adduct (blue). Bond lengths, shown in angstroms next to hydrogen bonds (dashed lines), are those found in molecule 1 and are similar in molecules 2−4, except where stated ([a]3.4 in m2, 3.2 in m4; [b]3.4 in m1, 3.3 in m3; [c]not in m4; [d]replaced by water in m2; [e]not in m3; [f]bond to symmetry molecule in m1 and m2). Hydrogen bonds shown in green only occur in molecules 1 and 3; those in magenta only occur in molecules 2 and 4. Catalytic residues Asn 106 and His 108 are shown in bold.

in conformation of residues Gln 170 and Glu 173. The result is that, in molecules 2 and 4, the C2 hydroxyl of the ribose hydrogen bonds to the main-chain carbonyl of Ile 107, while the C3 hydroxyl is hydrogen bonded to the side-chain carboxyl of Glu 173 (Figure 7). In molecules 1 and 3, the C2 hydroxyl forms a hydrogen bond to the carboxyl of Glu 173, and the C3 hydroxyl interacts with the side-chain amine of Gln 170 (Figure 7). Overall, the substrate portion of the adduct bears a striking resemblance to the conformation of β-GAR in the 5-DATHF structure, including the ribose ring pucker, which is more planar and disordered in the 10-formyl-TDAF-β-GAR complex. In particular, the glycine moiety superimposes well (Figure 6), with only a minor shift of 0.8 Å in the position of the primary amine, adding credence to the hypothesis that the structure observed in the 10-formyl-TDAF complex is a close structural mimic of the transition state of the formyl transfer reaction (*9*).

In each of the folate analogue structures, the plane of the pteridine portion is oriented at a slightly different angle. For example, the flexible pyrimidone of BW1476U89 adopts two distinct conformations with the plane of the ring varying by 16° (*7*). The quinazoline of the multisubstrate adduct is tilted by 12° and 9° relative to the 5-deazapterin of 5-DATHF and the quinazoline of 10-formyl-TDAF, which are orientated similarly (Figure 6). In addition, the quinazoline of the MAI is pulled down, toward the substrate, by 0.7 Å relative to the quinazoline of 10-formyl-TDAF, probably due to the formation of the covalent bond to the substrate, which is tightly anchored in the active site. Despite these differences, each compound presents similar hydrogen bond interactions to the backbone carbonyl of Leu 92 and the amide of Ile 91 (Figure 7). However, as a result of the change in conformation of the flexible 141−146 loop, two hydrogen bond interactions, from the main-chain carbonyl of Thr 140 to N3 and from the main-chain amide of Asp 144 to O4, have been lost. These ligand contacts with the protein main chain are replaced by new hydrogen bond interactions with bound water molecules that then set up an extensive local hydrogen-bonding network (Figure 7). This flexible loop has been described as a "folate-dependent" loop (*8*, *9*) and is normally responsible for the correct positioning of the catalytic residue Asp 144 when folate analogues are bound. In the structure presented here, the covalent multisubstrate adduct is formed in the active site and might be expected to more likely resemble the transition state rather than the substrate/cofactor bound states. However, only a spatial positioning of the reactive epoxide in close proximity to the primary amine of β-GAR is required for formation of the MAI and, hence, does not necessarily depend on the positioning of the catalytic residues, as in the enzyme reaction. So, perhaps in this structure, the 141−146 loop adopts a conformation that would, ordinarily, facilitate product release, after the catalytic steps have taken place.

As a result of covalent bond formation to β-GAR and/or repositioning of the quinazoline, the C10, benzoyl ring, and glutamate portion of the folate analogue are shifted toward Arg 64 relative to the parent 10-formyl-TDAF compound structure (1.36 Å between the C10 atoms, 1.28 Å between the Cα atoms). The orientation of the benzoyl ring is most similar to that of 5-DATHF. The most striking divergence occurs at the glutamate moiety (Figure 6). The glutamate carboxylate in the BW1476U89, 10-formyl-TDAF, and 5-DATHF (disordered) forms a salt bridge with Arg 64 and a hydrogen bond with the backbone amide of Ile 91. As a consequence of moving closer to Arg 64, the glutamate side chain and terminal carboxylate in this structure have swapped positions (Figure 7), and a salt bridge with Arg 64 and a hydrogen bond with the backbone amide of Ile 91 are now formed with the terminal carboxylate. The glutamate side chain is flexible, as evidenced in the electron density (Figure 3), and adopts a slightly different conformation in each of the four molecules. This alternative binding orientation for the glutamate may provide a better model for binding of the folate cofactor as the glutamate side chain, which becomes polyglutamated at the Cγ carbon, is pointing out of the binding pocket and can thus accommodate additional glutamate moieties.

A tightly bound water molecule close (2.7 Å) to the C10 hydroxyl (Figure 3) is capable of forming several hydrogen bonds to key active site residues such as His 108, Asn 106, and the primary amine of β-GAR (Figure 7). This water (W1) occupies a position similar to that of the side chain of Asp 144 in the "folate-bound" loop conformation and potentially fulfills the role of this residue in stabilizing the conformation of His 108 in the absence of Asp 144 due to the loop rearrangement. The multisubstrate adduct formed between the substrate and the dibromide (or its epoxide derivative) is firmly held in the active site of GAR Tfase through an extensive network of hydrogen bonds, involving both active site residues and numerous water molecules (Figure 7). Therefore, the effective inhibitory property of compound **1** is probably afforded by the MAI, while the time dependence of inhibition arises from the conversion of compound **1** to

the epoxide **2** and subsequent adduct formation within the enzyme active site.

Inhibition by the Epoxide. The epoxide **2** was assayed as a time-dependent inhibitor against GAR Tfase under conditions utilized for the assessment of dibromide **1** (*15*). Compounds **1** and **2** display almost identical, time-dependent inhibitory activity against GAR Tfase in the presence of the substrate β-GAR (Figure 2). In the absence of β-GAR, the potent, time-dependent GAR Tfase inhibitory activity was lost. Even in the absence of enzyme, but in the presence of β-GAR, compounds **1** and **2** behaved similarly and retained some activity, albeit significantly lowered, suggesting a small amount of adduct formation between β-GAR and **1** or **2**. The epoxide **2** and dibromide **1** appear to retain slight activity when the preincubation with the enzyme was conducted in the absence of the β-GAR. These results are consistent with the formation of the enzyme-assembled multisubstrate adduct inhibitor between compounds **1** or **2** and the substrate β-GAR that is observed in the X-ray studies rather than direct alkylation of the GAR Tfase active site. Compound **2** was also tested against DHFR (data not shown). After incubation with DHFR for 3 days, no loss of enzymatic activity was seen, indicating that compound **2** shows selectivity between DHFR and GAR Tfase.

The cytotoxic activity of compounds **1** and **2** against the CCRF-CEM cell line was tested in the presence and absence of added hypoxanthine (Table 2). To the extent that this could be established, the preformed epoxide **2** exhibited slightly more cytotoxic activity (ca. 2×) than the dibromide **1** against CCRF-CEM cells (IC_{50} > 10 μM). Neither exhibited a dependence on media purines [(+) and (−) hypoxanthine), indicating that the modest cytotoxic activity is not being derived from inhibition of purine biosynthesis characteristic of selective GAR or AICAR Tfase inhibition. However, such results can be attributed to inefficient cellular uptake or lack of polyglutamation, and therefore, further development of the inhibitor is required to improve its affinity for the cellular folate transport enzymes and folylpolyglutamyl synthetase.

Compound **2** has comparable, time-dependent enzymatic inhibitory properties to compound **1** (Figure 2). The conversion of the dibromide **1** to the epoxide **2** in weakly basic or buffered aqueous medium was established experimentally (Scheme 1), presumably via the intermediate bromohydrin as outlined in Scheme 2. Since compounds **1** and **2** exhibited nearly identical time-dependent inhibition of GAR Tfase, the in situ conversion of the dibromide **1** to the epoxide **2** in aqueous medium is so facile that it is not rate limiting in terms of the GAR Tfase time-dependent inhibitory activity. In addition, the MAI formed results from the reaction of one of the two epoxide diastereomers, the (10*S*) derivative, as established in the X-ray structure. It is unknown whether this is derived from selective binding of the (10*S*) derivative or subsequent selective reaction of the (10*S*) versus (10*R*) derivative with enzyme-bound β-GAR.

In conclusion, the crystal structure of the ternary complex of *E. coli* GAR Tfase, β-GAR, and 10-bromo-10-bromomethyl-5,8,10-trideazafolic acid, **1**, confirmed that the time-dependent inhibition of GAR Tfase is due to the formation of a multisubstrate adduct between the amine of β-GAR and the folate inhibitor in the enzyme active site. This discovery confirms that the efficacy of folate-based inhibitors can be enhanced by enzyme-catalyzed multisubstrate adduct formation with the substrate and, thus, should be pursued in future inhibitor design. More importantly, the structure revealed an unexpected and novel in situ conversion of **1** into the biologically active epoxide **2**. This unique and surprising in situ conversion to the biologically active form of the inhibitor explains the unusually effective properties of the dibromide **1**, which would not have been realized in the absence of the crystal structure, thus emphasizing the importance of crystallography in the iterative process of inhibitor design. With this example, we have shown that an epoxide, when properly presented to the β-GAR substrate amine, will react within the active site producing a potent MAI. With this proof of principle of epoxide-based inhibitors in hand, we are currently designing second generation inhibitors that will not only react with the substrate to form an MAI but also incorporate epoxides or aziridines that are more stable and potentially useful in vivo. The utilization of epoxides in inhibitor design has already been shown to be effective in a number of compounds, such as Rhizoxin, a novel antitumor antibiotic that inhibits microtubule assembly (*36*−*38*), and TNP-470, an angiogenesis inhibitor (*39*, *40*), both of which are presently in human clinical trials.

ACKNOWLEDGMENT

We thank the staff of Stanford Synchrotron Radiation Laboratory (SSRL) beam line 9-1 for helpful support, Mason Yamashita and Patricia Horton for protein purification, Michael Hedrick for performing the cytotoxic assay of the epoxide, and Markus Rudolph for useful discussions.

REFERENCES

1. Dev, I. K., and Harvey, R. J. (1978) *J. Biol. Chem. 253*, 4242−4244.
2. Inglese, J., Johnson, D. L., Shiau, A., Smith, J. M., and Benkovic, S. J. (1990) *Biochemistry 29*, 1436−1443.
3. Mueller, W. T., and Benkovic, S. J. (1981) *Biochemistry 20*, 337−344.
4. Boger, D. L., Haynes, N. E., Kitos, P. A., Warren, M. S., Ramcharan, J., Marolewski, A. E., and Benkovic, S. J. (1997) *Bioorg. Med. Chem. 5*, 1817−1830.
5. Almassy, R. J., Janson, C. A., Kan, C. C., and Hostomska, Z. (1992) *Proc. Natl. Acad. Sci. U.S.A. 89*, 6114−6118.
6. Chen, P., Schulze-Gahmen, U., Stura, E. A., Inglese, J., Johnson, D. L., Marolewski, A., Benkovic, S. J., and Wilson, I. A. (1992) *J. Mol. Biol. 227*, 283−292.
7. Klein, C., Chen, P., Arevalo, J. H., Stura, E. A., Marolewski, A., Warren, M. S., Benkovic, S. J., and Wilson, I. A. (1995) *J. Mol. Biol. 249*, 153−175.
8. Su, Y., Yamashita, M. M., Greasley, S. E., Mullen, C. A., Jennings, P. A., Warren, M. S., Benkovic, S. J., and Wilson, I. A. (1998) *J. Mol. Biol. 281*, 485−499.
9. Greasley, S. E., Yamashita, M. M., Cai, H., Benkovic, S. J., Boger, D. L., and Wilson, I. A. (1999) *Biochemistry 38*, 16783−16793.
10. Greasley, S. E., Horton, P., Ramcharan, J., Beardsley, G. P., Benkovic, S. J., and Wilson, I. A. (2001) *Nat. Struct. Biol. 8*, 402−406.
11. Bigham, E. C., Mallory, W. R., Hodson, S. J., Duch, D. S., Ferone, R., and Smith, G. K. (1993) *Heterocycles 35*, 1289−1307.
12. Inglese, J., Blatchly, R. A., and Benkovic, S. J. (1989) *J. Med. Chem. 32*, 937−940.
13. Sierra, E. E., and Goldman, I. D. (1999) *Semin. Oncol. 26*, 11−23.
14. Inglese, J., and Benkovic, S. J. (1991) *Tetrahedron 47*, 2351−2364.

15. Boger, D. L., Haynes, N. E., Warren, M. S., Ramcharan, J., Kitos, P. A., and Benkovic, S. J. (1997) *Bioorg. Med. Chem. 5*, 1839−1846.
16. Boschelli, D. H., Powell, D., Sharky, V., and Semmelhack, M. F. (1989) *Tetrahedron Lett. 30*, 1599−1600.
17. Ducruix, A., and Giege, R. (1992) *Crystallization of Nucleic Acids and Proteins: A Practical Approach*, Oxford University Press, New York.
18. Leslie, A. G. W. (1992) in *Joint CCP4 + ESF-EACBM Newsletter on Protein Crystallography*, CCP4, Daresbury Laboratory, Daresbury, Warrington, U.K.
19. Evans, P. R. (1997) in *Joint CCP4 + ESF-EACBM Newsletter on Protein Crystallography*, pp 22−24, CCP4, Daresbury Laboratory, Daresbury, Warrington, U.K.
20. Collaborative Computational Project, Number 4 (1994) *Acta Crystallogr. D 50*, 760−763.
21. Matthews, B. W. (1968) *J. Mol. Biol. 33*, 491−497.
22. Kissinger, C. R., Gehlhaar, D. K., and Fogel, D. B. (1999) *Acta Crystallogr. D 55*, 484−491.
23. Brünger, A. T., Adams, P. D., Clore, G. M., DeLano, W. L., Gros, P., Grosse-Kunstleve, R. W., Jiang, J. S., Kuszewski, J., Nilges, M., Pannu, N. S., Read, R. J., Rice, L. M., Simonson, T., and Warren, G. L. (1998) *Acta Crystallogr. D 54*, 905−921.
24. Jiang, J. S., and Brünger, A. T. (1994) *J. Mol. Biol. 243*, 100−115.
25. Brünger, A. T. (1992) *Nature 355*, 472−475.
26. Kleywegt, G. J. (1995) in *Joint CCP4 + ESF-EACBM Newsletter on Protein Crystallography*, pp 45−50, CCP4, Daresbury Laboratory, Daresbury, Warrington, U.K.
27. Jones, T. A., Zou, J. Y., Cowan, S. W., and Kjeldgaard, M. (1991) *Acta Crystallogr. A 47*, 110−119.
28. Cowtan, K. D., and Main, P. (1996) *Acta Crystallogr. D 52*, 43−48.
29. Laskowski, R. A., MacArthur, M. W., Moss, D. S., and Thornton, J. M. (1993) *J. Appl. Crystallogr. 26*, 283−291.
30. Inglese, J., Smith, J. M., and Benkovic, S. J. (1990) *Biochemistry 29*, 6678−6687.
31. Tutin, F., Caton, F. W., and Hann, A. C. O. (1909) *J. Chem. Soc. 95*, 2113−2127.
32. Hoering, P. (1905) *Chem. Ber. 38*, 3481−3488.
33. Guss, C. O. (1953) *J. Am. Chem. Soc. 75*, 3177−3179.
34. Guss, C. O. (1952) *J. Am. Chem. Soc. 74*, 2561−2563.
35. Hepworth, J. D., and Jones, T. K. (1981) *Tetrahedron 37*, 2613−2616.
36. Tolcher, A. W., Aylesworth, C., Rizzo, J., Izbicka, E., Campbell, E., Kuhn, J., Weiss, G., Von Hoff, D. D., and Rowinsky, E. K. (2000) *Ann. Oncol. 11*, 333−338.
37. McLeod, H. L., Murray, L. S., Wanders, J., Setanoians, A., Graham, M. A., Pavlidis, N., Heinrich, B., ten Bokkel Huinink, W. W., Wagener, D. J., Aamdal, S., and Verweij, J. (1996) *Br. J. Cancer 74*, 1944−1948.
38. Kaplan, S., Hanauske, A. R., Pavlidis, N., Bruntsch, U., te Velde, A., Wanders, J., Heinrich, B., and Verweij, J. (1996) *Br. J. Cancer 73*, 403−405.
39. Stadler, W. M., Kuzel, T., Shapiro, C., Sosman, J., Clark, J., and Vogelzang, N. J. (1999) *J. Clin. Oncol. 17*, 2541−2545.
40. Kruger, E. A., and Figg, W. D. (2000) *Expert Opin. Invest. Drugs 9*, 1383−1396.

BI011482+